Dicle University Journal of Engineering (DUJE)

web: http://dergipark.gov.tr/dumf

Research Article

Effect of rotor geometry on performance of 6/4 switched reluctance motors

Ahmet FENERCİOĞLU[1,*], Merve ŞEN KURT[2], Altan ŞAHİN[3], Zafer KELEŞ[4], Tuba KOCAER[5]

[1] Gaziosmanpaşa Üniversitesi, Mekatronik Mühendisliği Bölümü, Tokat, ORCID iD 0000-0002-1522-6868
[2] Amasya Üniversitesi, Elektrik Elektronik Mühendisliği Bölümü, Amasya, ORCID iD 0000-0003-1648-9368
[3] KORMAS Elektrikli Motor San. Tic. A.Ş., Kocaeli, ORCID iD 0000-0002-5041-4709
[4] KORMAS Elektrikli Motor San. Tic. A.Ş., Kocaeli, ORCID iD 0000-0002-0254-1068
[5] KORMAS Elektrikli Motor San. Tic. A.Ş., Kocaeli, ORCID iD 0000-0003-4614-7158

ARTICLE INFO

Article history:

Received 02 February 2021
Received in revised form 22 April 2021
Accepted 1 May 2021
Available online 22 June 2021

Keywords:

Switched Reluctance Motor, Rotor Geometry, Finite Element Method, Modelling

ABSTRACT

This study investigates the effect of rotor geometry on performance in switched reluctance motors (SRM) using models analyzed by the 2-D Finite Element Method (FEM). All models have the same stator geometry, winding features, and air gap, but have different rotor geometries. The SRM model operates at nominal speed of 3000 rpm; with 6/4 pole and 150 W output power. Magnetic model analysis was undertaken for the 3 different rotor models. Electrical performance characteristics; speed, phase current, source current, efficiency, electromagnetic torque, and load torque were determined. Magnetic flux density and flux lines in the stator and rotor and the current densities in windings are presented. The optimal rotor model for SRM was determined by considering electrical and magnetic performance data.

Doi: 10.24012/dumf.955418

Introduction

Switched Reluctance Motors (SRM) have become widely preferred in applications requiring high speed due to their superior characteristics including simple structure, low moment of inertia and high volume/power ratio. Their pole rotors do not contain structures such as collector, rings, magnets, brushes, or windings. In this way, the cost of the motor is decreased and the motor gains a robust and simple structure. In addition, the laminated rotor structure, which does not contain structures such as magnets or brushes, eliminates the decrease in efficiency caused by copper losses [1].

However, SRMs have disadvantages including vibration and noise due to the ripple in their torque [2]. Also, they require different driver circuits for different structures, and motion sensors for switch control [3,4].

In SRMs, the geometric structure of the motor directly affects the operating characteristics, and output parameters and the effect of factors, including pole arc width of rotor, air gap, skew angle of rotor and stator, stator/rotor pole number, pole embrace, and the truncation of pole corners, on SRM output performance have been investigated. In SRM, a change made to the rotor geometry leads to a change of rotor reluctance and inductance by affecting the flux path length and cross-section, which will affect torque and power in direct proportion to the square of the current [5].

The effect of the rotor pole angle on the electrical, mechanical and magnetic performance of the motor has been discussed in numerous studies [6-8]. The condition of the rotor pole arc being larger or smaller than the stator pole arc ($\beta_r > \beta_s$ and $\beta_s > \beta_r$) will change the reluctance of the magnetic circuit, which will lead to changes in inductance, input-output power, torque, and efficiency.

Please cite this article in press as A. Fenercioglu, M. Şen Kurt, A. Şahin, Z. Keleş, and T. Kocaer "Effect of rotor geometry on performance of 6/4 switched reluctance motors", DUJE, vol. 12, no. 3, pp. 459-469, June 2021.

Other modifications have been made to improve performance. For example, Lee at al. [9] modified the rotor to include a 2 mm hole in each rotor pole of an SRM of 13.5 kW, which reduced torque ripple by 4.4%.

Other studies have found the ratio of the stator/rotor pole number to be important to the performance of the SRM and have determined that as the ratio, N_s/N_r (N_s/N_r=6/4; 8/6; 12/8; 18/12), is increased, radial forces cause stator vibrations and noise is increased. It is further concluded that current and moment characteristics affect the power and moment densities and decrease moment ripple [10,11].

In SRM design, it is known that pole embrace, which is proportional to the number of stator/rotor poles, affects efficiency due to average torque. In a study where stator pole width ratio was fixed at 0.35 and rotor width ratio varied over the range 0.3-0.5, the highest torque, highest efficiency and lowest torque ripple were achieved for a rotor pole width ratio of 0.5. This suggests that pole width should be increased in applications where high torque, high efficiency, and low torque ripple are desired. However, when pole width is increased, cost increases proportionally. Therefore, when high power is required or performance increased, pole width should be increased [12].

Most studies focus on the effect of rotor geometry on torque and torque ripple. This study also investigates electrical performance characteristics including shaft speed, phase current, source current, efficiency, electromagnetic torque, and load. The study also develops a visual presentation of the magnetic flux density in the stator and rotor, flux lines, and current density in windings. A 6/4-pole SRM was selected to investigate the effect of 3 rotor geometries on motor performance using analytic techniques and finite element analysis. Results from the 2-dimensional finite element analysis will allow the best rotor model to be determined for applications in an axial and radial fan.

Materials and Methods

Switched Reluctance Motor (SRM)

When a current passes through a phase winding in a SRM, the torque in the motor will cause the rotor to move to the position of maximum inductance, resulting in rotation. If the rotor material is steel and there is no permanent magnetization, the direction of the current in the phase winding is not significant and the direction of torque is always towards the closest overlap position. In this way, the torque causes rotation in one direction, with movement occurring from the unaligned position to the aligned position, as shown in the sequence of the relative positions of rotor and stator in Figure 1 (a), (b), (c).

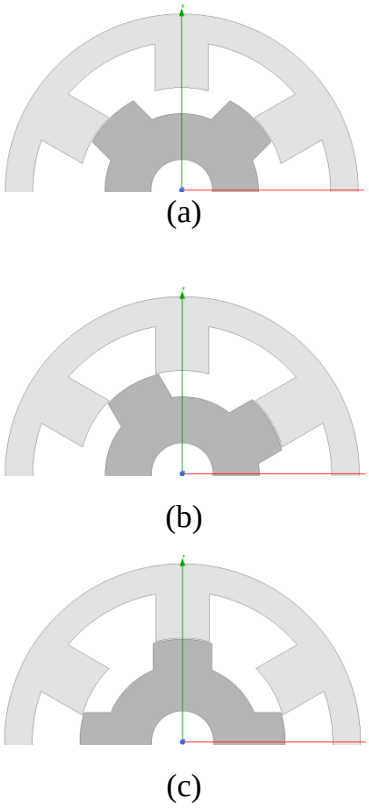

Figure 1. (a) Unaligned position, (b) Overlap position, (c) Aligned position

If the rotor and stator poles are symmetric, each phase can only generate torque in one direction according to the rotor pole arc angle. Therefore, at least two phases are needed to produce one-way torque in all rotor positions. If a current is passed through the winding while the rotor is rotating and it is in a position where the inductance is being reduced, a torque in an

opposing direction will be generated (known as braking or generator torque).

Torque ripple is high in SRMs. Smoother torque may be obtained by increasing the number of phases and including skew in the rotor. When the number of phases is increased, the electronic cost rises due to the greater number of switches in the driver. For low values of overall operating torque, the torque ripple in the three-phase motor can be reduced by the current profile. In practice, the phase current is reinforced in areas where there is torque descent [13-16].

SRM Magnetic Model

The SRM model investigated in this study has an output power of 150 W with a nominal maximum speed of 3000 rpm. The motor geometries that affect the performance of the SRM are shown in Figure 2 and defined in Table 1.

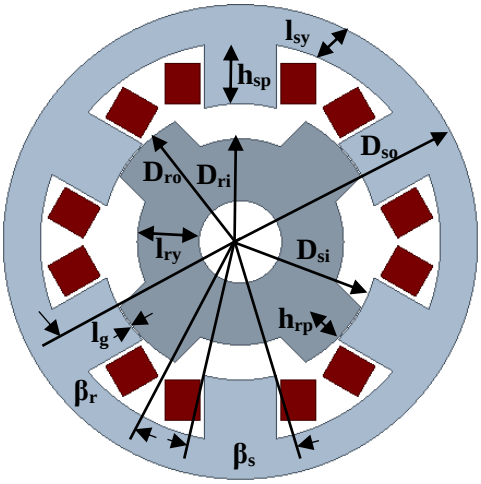

Figure 2. SRM cross-section parameters and dimensions

Table 1. Motor geometry parameters

Symbol	Quantity	Size
D_{so}	Stator outer diameter	115 mm
D_{si}	Stator inner diameter	67 mm
D_{ro}	Rotor outer diameter	66.3 mm
D_{ri}	Rotor inner diameter	20 mm
D_{sh}	Shaft diameter	10 mm
l_g	Air gap	0.35 mm
l_{sl}	Stack length	30 mm
β_s	Stator pole arc angle	30 deg
β_r	Rotor pole arc angle	33 deg
l_{sy}	Stator yoke length	9.5 mm
l_{ry}	Rotor yoke length	15 mm
h_{sp}	Stator pole height	14.5 mm
h_{rp}	Rotor pole height	8.15 mm

The stator pole arc angle (β_s) shown in Figure 2 is given by Equation 1, where n_s is the number of stator poles [17]. The rotor pole arc angle (β_r) (Equation 2) was made to be 10% greater than the stator pole arc angle to avoid a zero torque position.

$$\beta_s = \frac{\pi}{2n_s} \quad (1)$$

$$\beta_r = \beta_s \times 1.1 \quad (2)$$

The flux path cross-section at the rotor pole (A_r) is given by Equation 3, and the flux path cross-section at the stator pole (A_s) is given by Equation 4 [17]. The ratio of the stator outer diameter to the stack length is taken as (D_{so}/D_{sl}) = 3.83. In this case, the stack length is calculated as 30 mm.

$$A_r = D_{ro} \times \beta_r \times l_{sl} \quad (3)$$

$$A_s = (D_{ro} + l_g) \times \beta_s \times l_s \quad (4)$$

The stator yoke flux path cross-section (A_{sy}) is given by Equation 5, and the rotor yoke flux path cross-section (A_{ry}) is given by Equation 6, where l_{sy} and l_{ry} are the stator and rotor yoke length, respectively [17].

$$A_{sy} = l_{sy} \times l_{sl} \quad (5)$$

$$A_{ry} = l_{ry} \times l_{sl} \quad (6)$$

The mean flux path length at the stator (l_{fs}) is given by Equation 7 and the mean flux path length at the rotor (l_{fr}) is given by Equation 8. The stator pole length (h_{sp}) and rotor pole length (h_{rp}) in the related equations give the flux path length in the poles [17].

$$l_{fs} = 2h_{sp} + \frac{(D_{so}+D_{si})\times\pi}{2} \quad (7)$$

$$l_{fr} = 2h_{rp} + \frac{(D_{ro}+D_{ri})\times\pi}{2} \quad (8)$$

The SRM attempts to maximize the inductance in the active phase by triggering phase windings in an appropriate order to generate the moments of torque. The total reluctance (R_s) of the magnetic circuit must be considered when calculating the inductance in the active phase. The magnetic flux path formed in the SRM when current is applied to the stator windings is shown in Figure 3(a), with the equivalent magnetic circuit shown in Figure 3(b), and consists of the entire rotor and stator yokes. In the aligned position, the flux path cross-section of the rotor and stator poles is symmetric and flux flows equally along the two alternate paths around the stator.

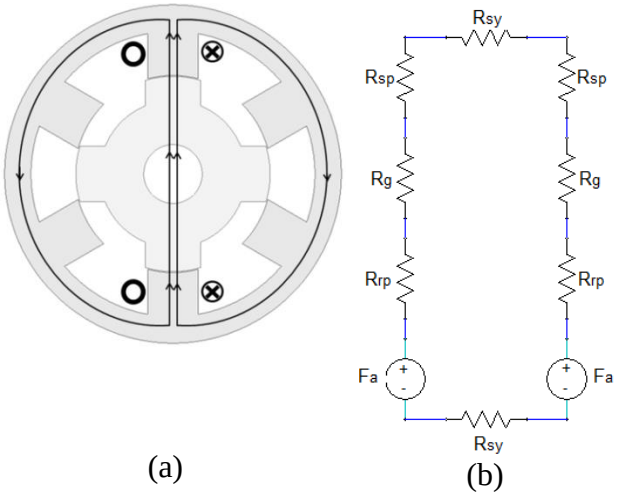

Figure 3. (a) Magnetic flux path (b) Magnetic equivalent circuit

The total reluctance (R_t) of the magnetic equivalent circuit is the sum of the stator pole reluctance (R_{sp}), stator yoke reluctance (R_{sy}), rotor pole reluctance (R_{rp}), rotor yoke reluctance (R_{ry}) and air gap reluctance (R_g), as shown in Equation 9 [17].

$$R_t = 2(R_{sp} + R_{rp} + R_g) + R_{sy} + R_{ry} \quad (9)$$

The total reluctance may be expressed in terms of the permeability, μ, of the materials, where μ_0 is the permeability of vacuum, as given in Equation 10.

$$\Sigma R = R_t = 2\left(\frac{h_{sp}}{\mu A_s} + \frac{h_{rp}}{\mu A_r} + \frac{l_g}{\mu_0 A_g}\right) + \frac{l_{fs}}{\mu A_{sy}} + \frac{l_{fr}}{\mu A_{ry}} \quad (10)$$

The phase inductance (L) is determined from the total reluctance, as in Equation 11, where N is the number of turns of the winding [17].

$$L = \frac{N^2}{\Sigma R} \quad (11)$$

The phase inductance of the SRM varies according to rotor position; with maximum phase inductance (L_a) occurring when rotor and stator pole are aligned, as shown in Figure 1 (c), and minimum phase inductance (L_u) occurring when rotor and stator poles begin to overlap, as shown in Figure 1 (b). In any unaligned position (Figure 1(a)) the inductance can be found for a given angle, θ, from Equation 12 [17].

$$L(\theta, i) = a_0 - a_1 \cos(n_r, \theta) \quad (12)$$

where n_r refers to the number of the rotor poles. The coefficients a_0 and a_1 are from the maximum and minimum inductances as Equation 13.

$$a_0 = \frac{L_{max}+L_{min}}{2}, a_1 = \frac{L_{max}-L_{min}}{2} \quad (13)$$

The electromagnetic torque (T) for rotor position is given by Equation 14. This indicates SRMs are capable of generating a high starting moment as the moment changes with the square of the current.

$$T(\theta, i) = \frac{1}{2} i^2 \frac{dL(\theta,i)}{d\theta} \quad (14)$$

Mean torque or electromagnetic torque (T_e) is given by Equation 15.

$$T_e = \frac{1}{2} i^2 \frac{L_a - L_u}{\beta_s} \quad (15)$$

Analysis Method

The 2-dimensional analysis of the motor and driver circuit was undertaken using Finite Element Method (FEM), using the ANSYS/Maxwell FEM software.Transient and steady state analysis was performed for 3 different rotor geometries, named Type-1, Type-2 and Type-3. Analysis was performed at a sampling frequency of 2000 Hz for 1.5 s, during which the motor speed changed from 0 rpm to a nominal maximum speed of 3000 rpm.

Model of the SRM

The rotor geometry of the 3 motor models used in this study, Type-1, Type-2 and Type-3, is shown in Figure 4 (a), (b) and (c). All models had the same stator geometry and air gap. The motor power was 150 W, operating voltage 26 V DC and nominal maximum motor speed 3000 rpm.

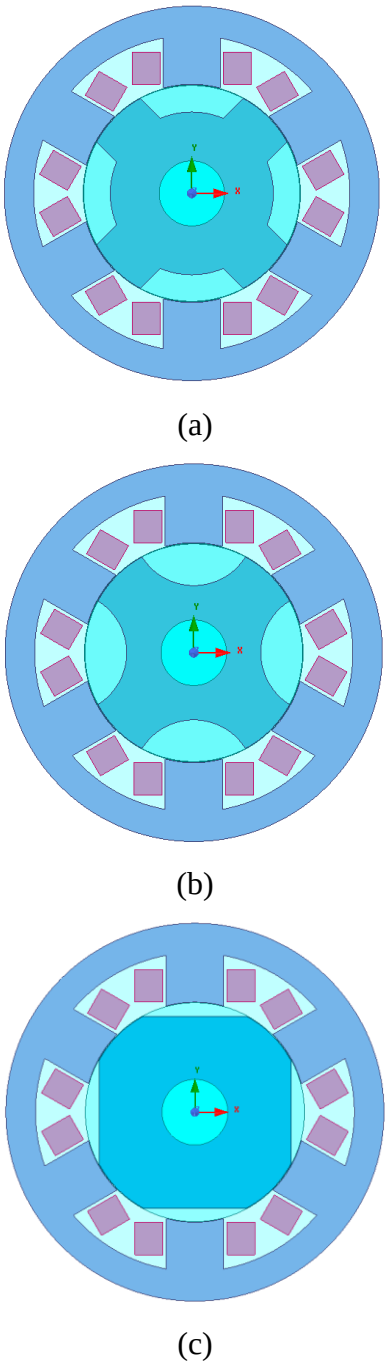

Figure 4. Rotor geometry types (a) Type-1, (b) Type-2, (c) Type-3

A siliceous steel with a stacking factor of 0.95 with B-H curve as given in Figure 5 was used as rotor and stator material.

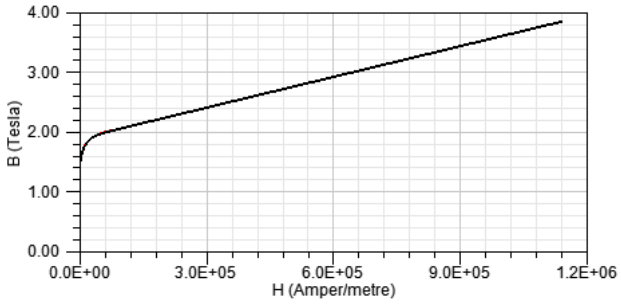

Figure 5. BH curve of the stator and rotor material

Driver Circuit

The 3-phase asymmetric bridge circuit given in Figure 6 was used to control the current in the 3 phases of the 6/4-pole SRM. Six (6) switching elements were used (two elements per phase), which ensured continuous rotation by switching the phases sequentially. The design of the rotor ensures that magnetic coupling between the phases is kept to a minimum, allowing independent control of each phase.

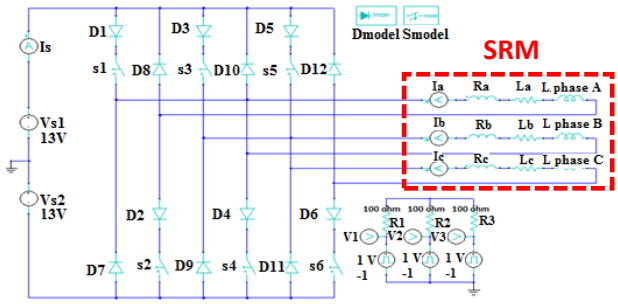

Figure 6. Driver circuit used in the simulation of the SRM

Finite Element Analysis (FEA)

Electrical and Mechanical Parameter

FEM was used for the 2-dimensional analysis of the SRM. Three (3) rotors having different shape, yoke length (l_{ry}), rotor height (h_{rp}) and rotor area (A_r) were modeled (Figure 4 (a), (b), (c)). Stator geometry, number of turns, conductor size, and motor lamination material were maintained the same in all analyses.

Figure 7 shows the speed for the three rotor geometries during the start-up transient state and the average speed for steady-state conditions. This shows the Type-3 rotor geometry to have an average speed that is lower than Type-1 and Type-2.

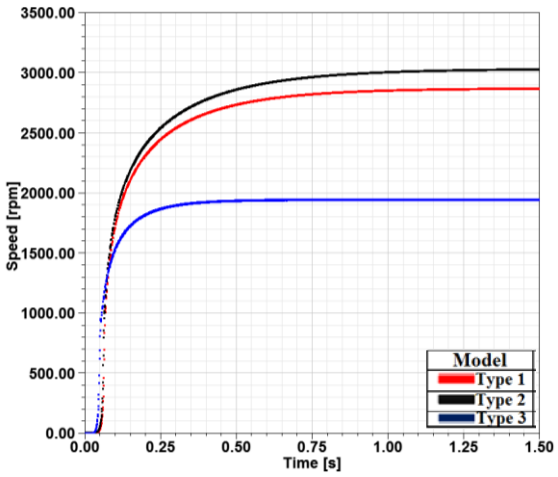

Figure 7. Speed depending on the rotor geometry

Figure 8 shows the variation in electromagnetic torque and load torque for the three rotor geometries in steady state. It is seen that the Type-3 rotor geometry maintains a higher electromagnetic torque compared to the Type-1 and Type-2 rotor geometries, resulting in electromagnetic torque and load torque that are approximately 40% higher. Figure 8 also shows that at rated speed there is no occurrence of negative electromagnetic torque during a phase. However note that the Type-3 rotor geometry reaches a lower final speed compared to the Type-1 and Type-2 rotor geometries.

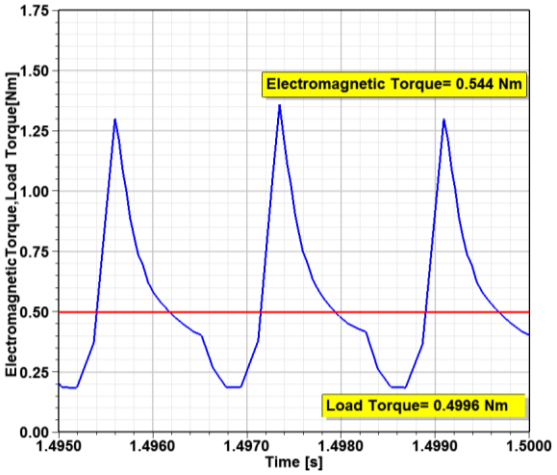

(a)

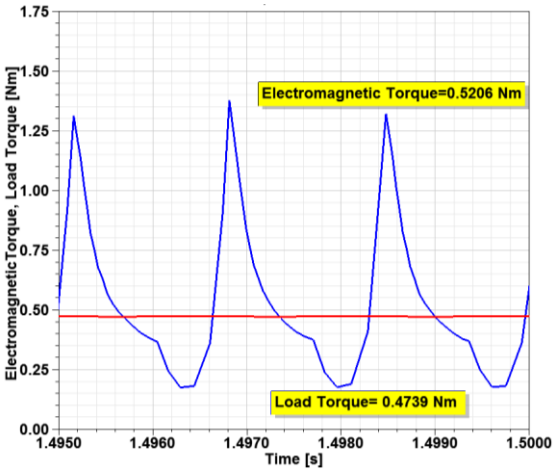

(b)

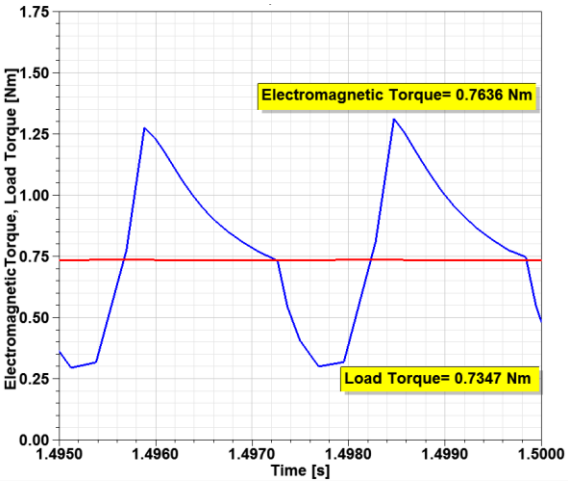

(c)

Figure 8. Electromagnetic torque and load torque depending on rotor geometry (a) Type-1, (b) Type-2, (c) Type-3

Table 2 presents the average and ripple values for electromagnetic and load torque in steady state for the 3 rotor geometries. This shows the Type-3 rotor geometry has higher average torque and lower ripple and should be preferred in applications where these are important.

Table 2. Average Torque and Torque Ripple depending on rotor geometry

	Electromagnetic Torque		**Load Torque**	
	Avg. [Nm]	**Ripple [SI]**	**Avg. [Nm]**	**Ripple [SI]**
Type-1	0.5437	57.996	0.4996	0.167
Type-2	0.5206	60.428	0.4739	0.226
Type-3	0.7636	40.822	0.7347	0.145

Figure 9 shows how the stator phase current (I) varies depending on the rotor geometry. In models with Type-1 and Type-2 rotor geometry, the effective value of the phase current is approximately 3.5 A, whereas it is 5.16 A in Type-3, which would account for the higher torque.

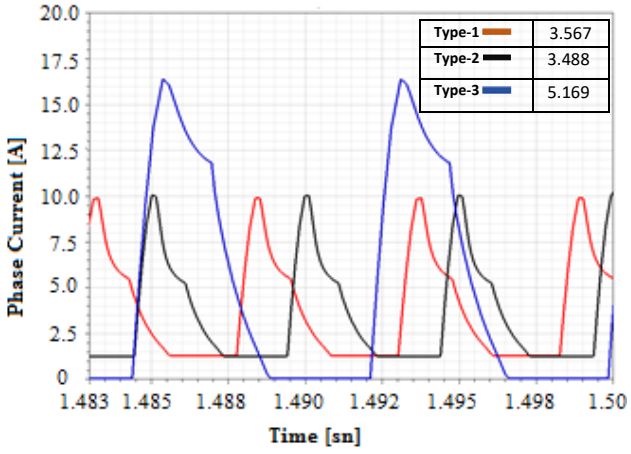

Figure 9. Phase current depending on rotor geometry

Figure 10 shows the source current (I_s) for each rotor geometry. The Type-1 and Type-2 rotor geometries have an effective source current, I_s, of 6.9 A, whereas the Type-3 has I_s of 7.55 A.

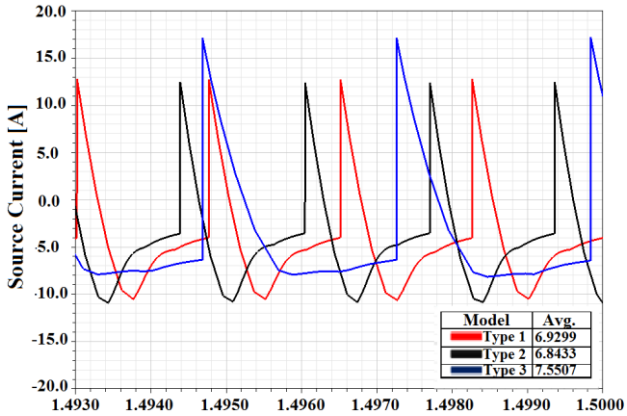

Figure 10. Source current depending on rotor geometry

Magnetic Parameters

The SRMs have been designed to operate with the core in saturation in order to achieve optimum performance. Figure 11 shows the distribution of flux lines with the rotor at an intermediate position, and how two poles occur.

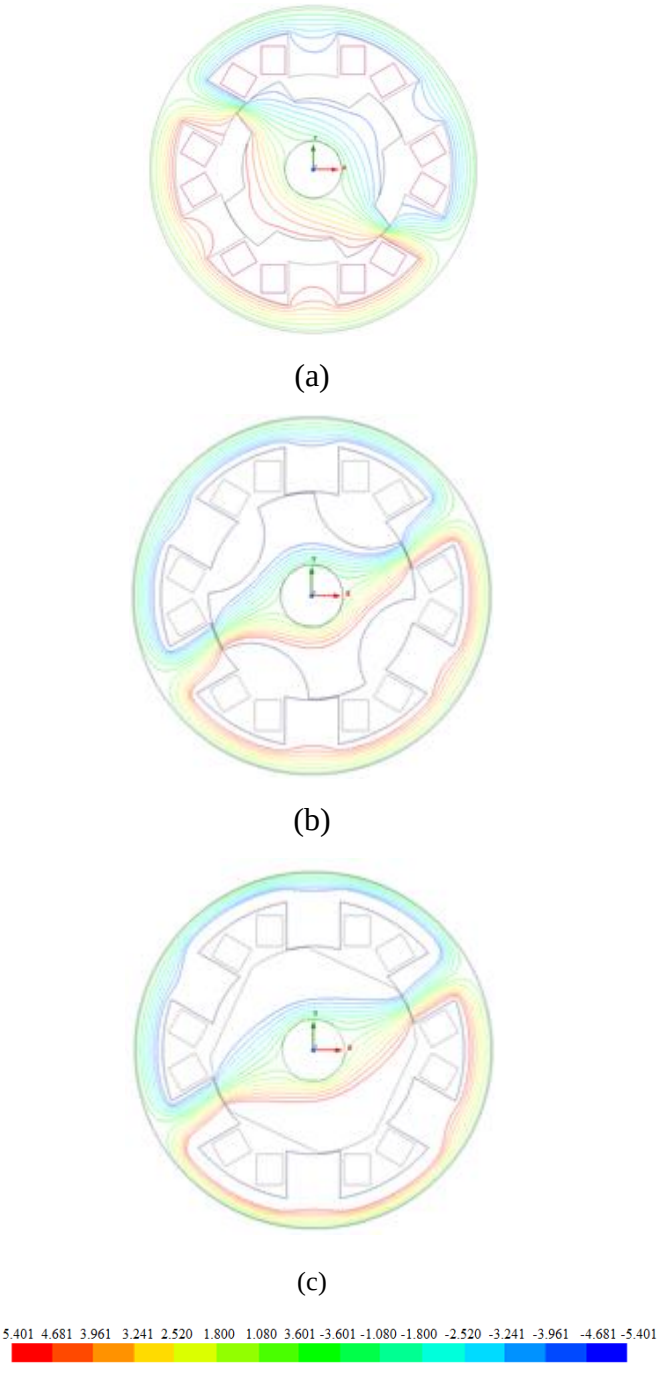

Figure 11. SRM flux lines (Wb/mm) (a) Type-1, (b) Type-2, (c) Type-3

It is recommended that the magnetic flux density in the stator, rotor tooth and yoke regions of an SRM should be less than 1.8 T [18]. Figure 12 shows the distribution of the magnetic flux density in the stator and rotor in steady state for the Type-1, Type-2 and Type-3 rotor geometries.

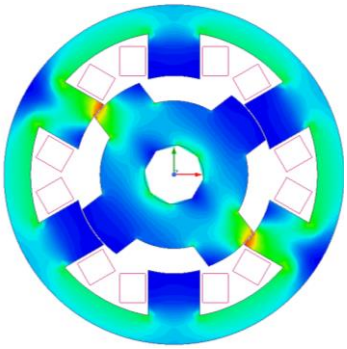

(a)

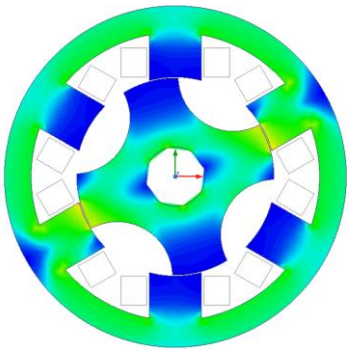

(b)

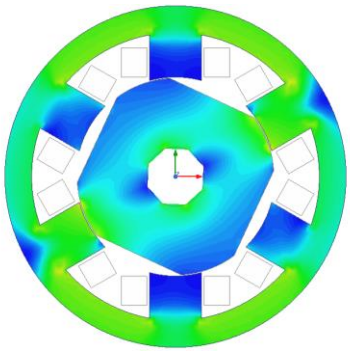

(c)

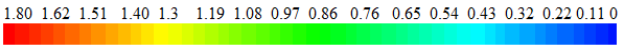

Figure 12. SRM magnetic flux density distribution (T) (a) Type-1, (b) Type-2, (c) Type-3

The maximum value for the magnetic flux density in the various regions of the stator and rotor for 3 geometries are given in Table 3 and shows that the magnetic flux density does not exceed the recommended maximum value in any location [18].

Table 3. Maximum magnetic flux density for the rotor geometries

	Stator Yoke	Stator Teeth	Rotor Yoke	Rotor Teeth
Type-1	0.634 T	1.650 T	0.694 T	1.510 T
Type-2	0.779 T	1.380 T	0.809 T	1.250 T
Type-3	1.080 T	1.344 T	0.871 T	1.209 T

Current Density in Stator Windings

In enclosed and naturally cooled electrical machines, the current density in the phase windings should be in the range $1.5 < J_b < 5$ A/mm^2 [19]. Figure 13 shows the distribution of the current density passing through the rotor bars at t = 1 sec. The current density of the stator phase windings in each of the 3 geometries remains within the allowed range and indicates forced cooling is not needed.

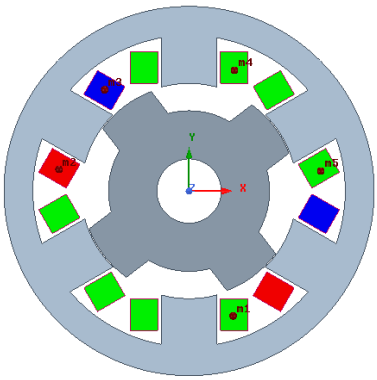

Name	X	Y	Z	J
m1	13.664	-38.892	0.000	-6.149e+00
m2	-40.422	6.752	0.000	4.801e+06
m3	-26.175	31.552	0.000	-4.801e+06
m4	14.079	37.600	0.000	-6.149e+00
m5	40.892	6.229	0.000	-7.384e+03

Time =1.40000832000002s
Speed =2863.694170rpm
Position =262.390619deg

(a) max 4.8 A/mm^2

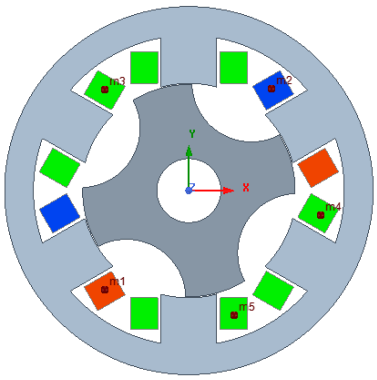

Name	X	Y	Z	J
m1	-26.244	-30.963	0.000	3.996e+06
m2	25.768	31.849	0.000	-3.996e+06
m3	-26.244	31.564	0.000	-6.147e+00
m4	41.116	-7.657	0.000	-6.147e+00
m5	14.115	-38.921	0.000	-6.177e+00

Time =1.40001976000002s
Speed =3019.634722rpm
Position =239.999922deg

(b) max 3.99 A/mm^2

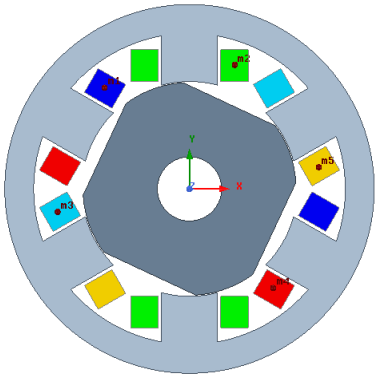

Name	X	Y	Z	J
m1	-26.433	31.593	0.000	-6.798e+06
m2	14.105	38.682	0.000	-6.240e+00
m3	-41.053	-7.173	0.000	-2.684e+06
m4	26.068	-30.876	0.000	6.798e+06
m5	40.245	6.783	0.000	2.684e+06

Time =1.39991472000002s
Speed =1943.460449rpm
Position =244.939341deg

(c) max 6.79 A/mm^2

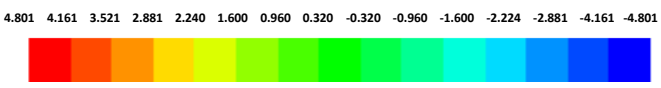

Figure 13. Current Density in Stator Windings (a) Type-1, (b) Type-2, (c) Type-3

CONCLUSION

In Switched Reluctance Motors, the rotor geometry directly affects the electrical and magnetic parameters, and thus performance. Changes only in rotor profile will alter the magnetic flux path length and cross-section, and thus the magnetic reluctance. This will change the inductance, which will result in a change in current, input power, and therefore efficiency.

In the Type-1 and Type-2 rotor geometries, the rotor pole and tooth geometry are arc-shaped, resulting in similar input power and efficiency. In the Type-3 rotor geometry, the edges of the rotor pole are flat and it has sharp points at the poles. This results in a higher input power and thus lower efficiency. This would compare with the findings of others; where the Type-2 rotor geometry with circular rotor pole and tooth geometry provide highest efficiency, but the Type-3 rotor geometry, with rotor pole and tooth geometry having rectangular shape and sharp points, gives the lowest efficiency.

A summary of the performance parameters is given in Table 4.

Table 4. Performance parameters of the rotor geometries

Motor Parameters	**Type-1**	**Type-2**	**Type-3**
Source Current, I_s (A)	6.93	6.84	7.55
Phase Current, I_p (A)	4.51	4.45	7.86
Speed, n (rpm)	2861	3018	1943
Load Torque, T_l (Nm)	0.50	0.47	0.73
Shaft Torque, T_m (Nm)	0.54	0.52	0.76
DC Feeding, V (V)	26.00	26.00	26.00
Core Losses, P_{fe} (W)	9.72	9.65	12.06
Copper Losses, P_{cu} (W)	9.15	8.91	27.80
Mechanical Losses, P_m (W)	10.00	10.00	7.00
Leakage losses, P_l (%1.5)	2.24	2.24	2.24
Output Power, P_o (W)	149.43	149.41	149.47
Output Power, P_i (W)	180.54	177.97	196.34
Efficiency, η (%)	82.77	83.95	76.13
Current Density, J (A/mm^2)	6.27	6.25	6.72
Flux linkage,λ (Wb)	0.01	0.0956	0.0147
Phase resistance, R_p (Ω)	0.15006	0.15006	0.15006

The Type-3 SRM has lower torque ripple than the other types due to having no-salient pole, therefore its mechanical losses are assumed as 7 W, as winding losses are low. Mechanical loss in the other types is assumed as 10 W.

Considering all electrical and mechanical performance parameters in Table 4, the Type-2

rotor geometry is optimal for the 3 phase 6/4 SRM.

Acknowledgement: This paper is derived from the project "Switched Reluctance Motor and Driver for Axial Fans and Blower Applications" undertaken in KORMAS R&D Center and supported by TUBITAK Teydeb project 7180878. A summary Turkish version of this paper was presented in EEMKON 2019 Congress.

References

1. C.E. İyde, A. Polat, L. T.Ergene, "6/4 ve 8/6 stator/rotor yapılarında ARM tasarımı, analizi ve karşılaştırması," *Paper Presented at the National Conference on Electrical, Electronics and Biomedical Engineering*, 2016, pp. 339–343.
2. Ü. Mutlu, "Anahtarlamalı Relüktans Motor Sürücü Devre Tasarimi," Msc Thesis, Institute of Science and Technology, Erciyes, 2006.
3. M.M. Alaee, E. Afjei., S. Ataei, "A new resonant driver for switched reluctance motor," *Paper Presented at the International Conference on Electrical Engineering*, 2007.
4. K. Masoudi, M.R. Feyzi., A. Masoudi, "Reduction of vibration and acoustic noise in the switched reluctance motor by using new improved stator yoke shape," *Paper Presented at the 21st Iranian Conference on Electrical Engineering*, 2013, pp. 1–4.
5. Bal G., *Özel Elektrik Makinaları*, Seçkin Press, 2011, Ankara.
6. B. Bilgin., A. Emadi., M. Krishnamurthy, "Design considerations for switched reluctance machines with a higher number of rotor poles," *IEEE Trans. on Ind. Electronics*, vol. 59, no. 10, pp. 3745–3756, 2012.
7. A. Fenercioğlu & İ. Tarımer, "Anahtarlamalı relüktans motor tasarımlarında farklı rotor geometrilerinin motor güç ve tork üretimine etkileri," *Journal of Balıkesir University,* vol. 10, no. 1, pp. 19-30, 2008.
8. K. Vijayakumar et al., "Switched reluctance motor modelling, design, simulation, and analysis: a comprehensive review" *IEEE Transactions on Magnetics*, vol. 44, no. 12, pp. 4605–4617, 2008.
9. J.W. Lee et al., "New rotor shape design for minimum torque ripple of SRM using FEM," *IEEE Transactions on Magnetics*, vol. 40, no. 2, pp. 754 – 757, 2004.
10. P.C. Desai et al., "Switched reluctance machines with higher rotor poles than stator poles for ımproved output torque characteristics," *Paper presented at the 35th annual conference of IEEE industrial electronics*, 2009, pp. 1338–1343.
11. Z. Omaç, H. Kürüm, A.H. Selçuk., "18/12 kutuplu bir anahtarlı relüktans motorun tasarımı, incelenmesi ve kontrolü" *Fırat University Journal of Engineering Science*, vol. 19, no. 3, pp. 339-346, 2007.
12. A.V. Reddy & B.M. Kumar, "Torque ripple minimization of switched reluctance motor using pole embrace and pole configuration methods" *International Journal of Applied Engineering Research*, vol. 13, no. 10, pp. 8525-8529, 2018.
13. K. Çakır & A. Sabonovic, "In-wheel motor design for electric vehicles," *Paper Presented at the 9th International Workshop on Advanced Motion Control*, 2006, pp. 613-618.
14. T.W. Ng, K.W.E. Cheng, X.D., "Computation of the in-wheel switched reluctance motor inductance using finite element method," *Paper Presented at the 3rd International Conference on Power Electronics Systems and Applications*, 2009.
15. M.C. Tsai, C.C. Huang, Z.Y. Huang, "A new two-phase homopolar switched reluctance motor for electric vehicle applications," *Journal of Magnetism and Magnetic Materials*, vol. 267, no. 2, pp. 173-181. 2003.
16. M. Zeraoulia, M.H. Benbouzid, D. Diallo, "Electric motor drive selection issues for HEV propulsion systems: a comparative study," *IEEE Transactions on Vehicular Technology*, vol.55, no. 6, pp. 1756-1764, 2006.
17. A. Fenercioğlu & M. Dursun, "Design and analysis of outer rotor in-wheel motor," *International Review of Electrical Engineering*, vol. 6, no. 2, pp. 7545-751. 2011.
18. Z. Xu, D.H. Lee, J.W. Ahn, "Design of a novel 6/5 segmental rotor type switched reluctance motor," *Paper presented at the IEEE industry application society annual meeting*, 2014, pp 1-7.
19. Y. Yaşa, Y. Sözer, M. Garip, "High power density switched reluctance machine development for high-speed spindle applications,". *Turkish Journal of Electrical Engineering & Computer Sciences*, vol. 26, no. 2, pp. 1572 – 1586, 2018.